PHYSICAL REVIEW D VOLUME 25, NUMBER 11 1 JUNE 1982

# Topological, total, and elastic cross sections for $K^+p$, $\pi^+p$, and $pp$ interactions at 147 GeV/$c$

D. Brick, H. Rudnicka, A. M. Shapiro, and M. Widgoff
*Brown University, Providence, Rhode Island 02912*

R. E. Ansorge, W. W. Neale, D. R. Ward, and B. M. Whyman*
*University of Cambridge, Cambridge, England*

R. A. Burnstein and H. A. Rubin
*Illinois Institute of Technology, Chicago, Illinois 60616*

E. D. Alyea, Jr.
*Indiana University, Bloomington, Indiana 47401*

L. Bachman,† C. -Y. Chien, P. Lucas,‡ and A. Pevsner
*Johns Hopkins University, Baltimore, Maryland 21218*

J. T. Bober, R. Dolfini,§ T. Frank, E. S. Hafen, P. Haridas, D. Huang,|| R. I. Hulsizer, V. Kistiakowsky, P. Lutz,¶ S. Noguchi,** S. H. Oh, I. A. Pless, T. B. Stoughton, V. Suchorebrow, S. Tether, P. C. Trepagnier,†† Y. Wu,|| and R. K. Yamamoto
*Laboratory for Nuclear Science and Department of Physics, Massachusetts Institute of Technology, Cambridge, Massachusetts, 02139*

F. Grard, J. Hanton, V. Henri, P. Herquet, J. M. Lesceux, P. Pilette, and R. Windmolders
*Université de l'Etat, Mons, Belgium*

H. DeBock, F. Crijns, W. Kittel, W. Metzger, C. Pols, M. Schouten, and R. Van de Walle
*University of Nijmegen, Nijmegen, Netherlands*

H. O. Cohn
*Oak Ridge National Laboratory, Oak Ridge, Tennessee 37830*

G. Bressi, E. Calligarich, C. Castoldi, and S. Ratti
*University of Pavia and Istituto Nazionale di Fisica Nucleare, Pavia, Italy*

R. DiMarco, P. F. Jacques, M. Kalelkar, R. J. Plano, P. Stamer,‡‡ and T. L. Watts
*Rutgers University, New Brunswick, New Jersey 08903*

E. B. Brucker, E. L. Koller, and S. Taylor
*Stevens Institute of Technology, Hoboken, New Jersey 07030*

L. Berny, S. Dado, J. Goldberg, and S. Toaff
*Technion, Haifa, Israel*

G. Alexander, O. Benary, J. Grunhaus, R. Heifetz, and A. Levy
*Tel-Aviv University, Tel-Aviv, Israel*

W. M. Bugg, G. T. Condo, T. Handler, E. L. Hart, and A. H. Rogers
*University of Tennessee, Knoxville, Tennessee 37916*

Y. Eisenberg, D. Hochman, U. Karshon, E. E. Ronat, A. Shapira, R. Yaari, and G. Yekutieli
*Weizmann Institute of Science, Rehovot, Israel*

 

T. Ludlam,[§§] R. Steiner, and H. Taft
*Yale University, New Haven, Connecticut 06520*
(Received 2 December 1981)

The Fermilab hybrid 30-in. bubble-chamber spectrometer was exposed to a tagged 147-GeV/$c$ positive beam containing $\pi^+$, $K^+$, and $p$. A sample of 3003 $K^+p$, 19 410 $pp$, and 20 745 $\pi^+p$ interactions is used to derive $\sigma_n$, $\langle n \rangle$, $f_2^{cc}$, and $\langle n_c \rangle / D$ for each beam particle. These values are compared to values obtained at other, mostly lower, beam momenta. The overall dependence of $\langle n \rangle$ on $E_a$, the available center-of-mass energy, for these three reactions as well as $\pi^- p$ and $pp$ interactions has been determined.

## I. INTRODUCTION

This paper presents the total, elastic, and topological cross sections for $K^+p$, $\pi^+p$, and $pp$ interactions at 147 GeV/$c$. The Fermilab 30-in.-bubble-chamber—proportional-wire-chamber hybrid system was exposed to a meson-enriched tagged positive beam which produced a total of 400 000 frames from two separate runs.

The topological cross sections and multiplicity moments are based on 3003 $K^+p$ interactions, 20 745 $\pi^+p$ interactions, and 19 410 $pp$ interactions. Selected subsets of these events were used to determine the total and elastic cross sections in order to remove as much systematic bias as possible. Preliminary results of the above, based on a small fraction of these data, have been presented previously.[1]

Section II of this paper describes the beam line, detection equipment, and meson-enrichment techniques used. Section III is a presentation of the procedures used to extract the elastic and total cross sections from these data. The topological cross sections are determined in Sec. IV and the results obtained are compared with similar reactions, mostly at lower energies.

## II. EXPERIMENTAL PROCEDURE

### A. Apparatus

The arrangement of the essential components for this experiment are shown schematically in Fig. 1. The system consists of the Fermilab 30-in. hydrogen-filled bubble chamber providing a visible target augmented by beam-tagging Čerenkov counters ($C106$,$C108$), proportional wire chambers (PWC's) upstream ($A-C$) and downstream ($D-G$) from the bubble-chamber and chamber-trigger scintillation paddles (SC1,SC2). Downstream from these detectors the muon contamination was monitored by three plastic scintillators (MU1,MU2,MU3) behind 1 m of lead and a total 3.7 m of shielding concrete. All counter and chamber data were grouped according to arrival times of the beam particle during a beam spill. These components were used in previous experiments and have been described elsewhere.[2] New or improved components consist of a hadron filter in the beam line and prototype forward $\gamma$ detector. The forward $\gamma$ detector consisted of five F-2 Pb-glass bars in each

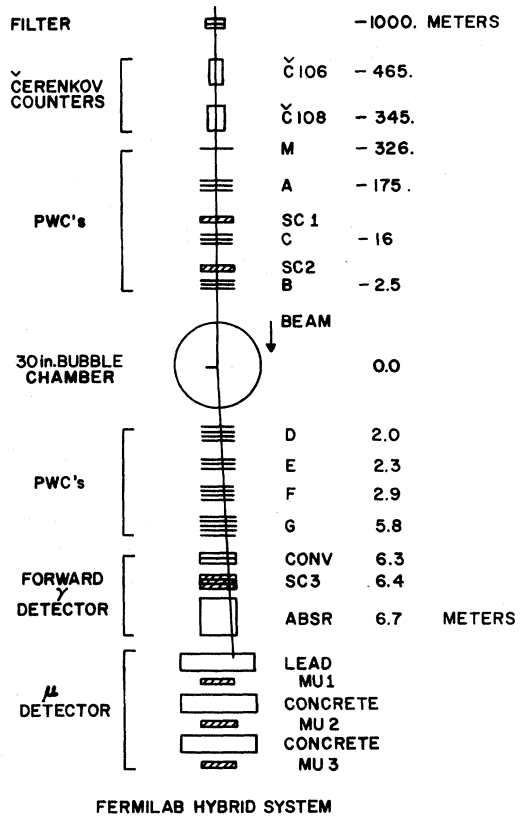


FIG. 1. Schematic diagram for the Fermilab hybrid 30-in. bubble-chamber spectrometer showing the locations of the upstream and downstream components. Typical trajectories of the particles from a two-prong event are indicated.

of two layers to initiate showers. The transverse profile was then sampled by a scintillator hodoscope and the electromagnetic energy of the shower was absorbed in additional Pb-glass. The detector was incorporated in the second of the two parts of this experiment with the results reported by Heller *et al.*[3]

The hadron filter was a very important addition to the beam line. With circulating protons at 400 GeV/$c$ impinging on a copper target, a 147-GeV/$c$ positive secondary beam at a production angle of 4 mrad is expected to contain approximately 78% protons, 16% pions, but only 1% kaons with the remainder consisting of muons. To improve the $K^+$ content the secondary beam was "filtered" through an absorber of low atomic weight.[4] More protons are scattered out of the beam that pions and more pions are scattered out than kaons because of the differing cross sections. This scattering thus should improve the $\pi/p$ and $K/p$ ratios. A 100-in.-long reservoir of water was interposed in the secondary beam upstream of $C106$ for the first part of the experiment (hereinafter called part I). The beam composition as monitored by the Čerenkov counters[5] and the upstream PWC's is given in Table I. A total of 145 000 frames were acquired in this portion of the experiment.

Following the completion of this part of the experiment, studies were undertaken to improve the $K^+$ component of the beam.[6] The second phase of the experiment used 15 ft of polyethylene as the filter. Each end of the filter could be moved independently perpendicular to the beam direction. This motion allowed for adjustment of the transverse position of the filter as well as its effective length.[7]

Approximately 250 000 frames were taken with the beam composition shown in Table I. The improvement in the $K^+$ content of the beam attained by using the polyethylene filter is readily apparent. This second portion of the experiment (part II) also had a higher average incident beam level of 6.46 tracks/frame compared to 4.76 tracks/frame for part I. Therefore, over 85% of the $K^+$ interactions in this experiment are contained in the part II film.

TABLE I. Beam composition in percent.

| Particle | Filter: Water | Filter: Polyethylene |
|---|---|---|
| $p$ | 56.96±0.44 | 29.03±0.17 |
| $\pi^+$ | 30.76±0.32 | 54.04±0.23 |
| $K^+$ | 3.70±0.11 | 9.78±0.10 |
| $\mu^+$ | 2.66±0.10 | 4.01±0.06 |
| Noise | 5.92±0.14 | 3.13±0.06 |

### B. Scanning

A common set of scan rules was adopted prior to the scanning of the film by the institutions involved. Provision was made to have the scan data, as well as any measurements, presented on magnetic tape in a form[8] that could be easily exchanged among the various institutions. All events within a predetermined fiducial volume were recorded except when (1) one or more views were missing or black, (2) any event was faint because of low bubble density, (3) there were too many incident tracks (both primary and secondary), or (4) there were more than two events within the fiducial volume. All of the above criteria for rejection are event-type independent. Care was taken to eliminate, or at least minimize, any event-type-dependent rejection which could introduce a bias into the sample. For each primary interaction in the fiducial volume, a complete description of the event as to the number of charged secondary tracks, $V^0$'s, $\gamma$'s, scatters, interactions, decays, etc., was recorded. An independent determination of the event description for each event was made and any differences were normally adjudicated by a physicist. The detailed procedure for this check and correction of the first scan was left to the individual institutions involved.

A second scan of the film, completely independent, was performed on at least 10% of the frames scanned by each institution. Single scan efficiencies were computed for each institution as a function of secondary multiplicity. These single scan efficiencies averaged 90.4% for two-pronged events. The scan efficiency for the higher multiplicities varied between 95.5% and 100% and averaged 96.7%.

### C. Event reconstruction

All good events were precision measured to be reconstructed in space. The measuring approach varied with institution as did the sequence of reconstruction programs used. The majority of the data was processed, eventually, through the PRECIS-GEOHYB sequence.[9] For this paper, however, a vertex-guidance-point measurement with an image-plane digitizer was sufficient for event selection.

#### 1. Beam tag

In principle, an interaction vertex in the bubble chamber may be associated with a unique beam track that has been reconstructed with a trajectory determined by the upstream PWC's and tagged by the Čerenkov counters. To be associated with a vertex any PWC track must have an impact parameter less than 1.25 mm in space with respect to the measured primary vertex.

Any event which had no beam track within the specified impact distance was discarded—13.5% of the interactions. In addition, 0.5% of the primary vertices could not be reconstructed in space.

The two Čerenkov counters offered some redundancy in the beam tag. The gas pressure in each Čerenkov counter was adjusted to provide $\pi$ and $K$ signals while protons remained below the threshold. One Čerenkov counter was segmented such that the light from the kaons illuminated an inner mirror and the pions an outer one. Only the three combinations of signals corresponding to the "legitimate" particle tags for $p$, $K^+$, or $\pi^+$ were accepted. All other combinations are ignored and lumped together as "noise" in Table I.

#### 2. Fiducial volume and beam count

The positions of the measured primary vertices were used to compute an average potential path length of a beam track through the fiducial volume. The scan volume had been chosen so as to have the primary vertex visible in all three views and to leave sufficient length in the chamber to measure adequately the secondary tracks. Assuming all beam tracks were parallel with a dip and azimuth angle determined by the upstream PWC's, the average potential path of an incident beam particle was calculated to be $40.5 \pm 0.2$ cm.

In every tenth frame, all beam tracks were reconstructed in the upstream PWC's and projected towards the bubble chamber to determine an average beam count. This average beam count was combined with the total number of usable frames to determine a total beam flux at the entrance window of the bubble chamber.

## III. ELASTIC, INELASTIC, AND TOTAL CROSS SECTIONS

The data used in the calculation of the elastic, inelastic, and total cross sections are based on a 56-roll subsample of part II film. These rolls contain 1597 $K^+p$ interactions, 10 665 $\pi^+p$ interactions and 9294 $pp$ interactions. All events were corrected for scan efficiency, reconstruction failure (no vertex), and random tape losses. A more severe correction was necessary for the two-prong sample.

### A. Elastics

#### 1. Separation of events

To separate the elastic events from the inelastic events two separate approaches were used. Kinematic fits to the elastic scattering hypotheses were attempted, by beam type, for all two-pronged events using a modified version of SQUAW. The second approach was to use the recoiling target proton to predict the direction and momentum of the scattered beam particle, assumed to be elastic, which was then projected through the chamber magnetic field to the location of the last downstream PWC chamber. The predicted location of the track was compared to the observed location of all possible impacts in this chamber. No significant differences between the two approaches were observed. A more detailed discussion of a similar comparison may be found in Ref. 2. An event was called an elastic scattering when $(Y_{\text{pred}} - Y_{\text{obs}})^2 + (Z_{\text{pred}} - Z_{\text{obs}})^2 \leq 10$ mm$^2$. With this criterion the fraction of two-pronged events fitting the elastic-scattering hypothesis were $0.52 \pm 0.02$ for $K^+p$, $0.56 \pm 0.02$ for $\pi^+p$, and $0.54 \pm 0.02$ for $pp$ interactions.

#### 2. Corrections

Not only do the two-prong events have a lower scan efficiency but they are prone to additional losses and biases. A scatter plot of the four-momentum transfer against the azimuthal angle of the scattered target for the elastic events displayed a depletion of events at low $t$, in particular when the azimuthal angle is parallel to the optic axis. For $|t| > 0.08$ the depletion disappears. The histograms of the $t$ distributions for the $pp$, $\pi^+p$, and $K^+p$ elastics are displayed in Figs. 2(a), 2(b), and 2(c), respectively. Each of these histograms was fitted to an exponential of the form $Ae^{bt}$ in the range $0.08 < |t| < 0.40$ (GeV/$c$)$^2$, with the best-fit slope listed in Table II. The results for the $\pi^+p$ and $K^+p$ slopes determined here agree within one

standard deviation (SD) with the counter results of Carroll *et al.*[10] and the Fermilab Single Arm Spectrometer Group.[11] Although not statistically significant the larger difference between the measured *pp* slopes (2.23 SD) could be attributed to the presence of a residual $\pi$ component due to beam inefficiencies. However, to attribute the entire difference to a $\pi$ component is unreasonable since that would require over a 50% $\pi$ contamination.

The fitted slopes were extrapolated to $t=0$ to yield an estimate of the missing low-$|t|$ events in the range $0<|t|<0.08$ (GeV/$c$)$^2$. It is estimated that 16% of $K^+$ scatters, 19% of $\pi^+$ scatters, and 32% of the *pp* elastic scatters were missed. The

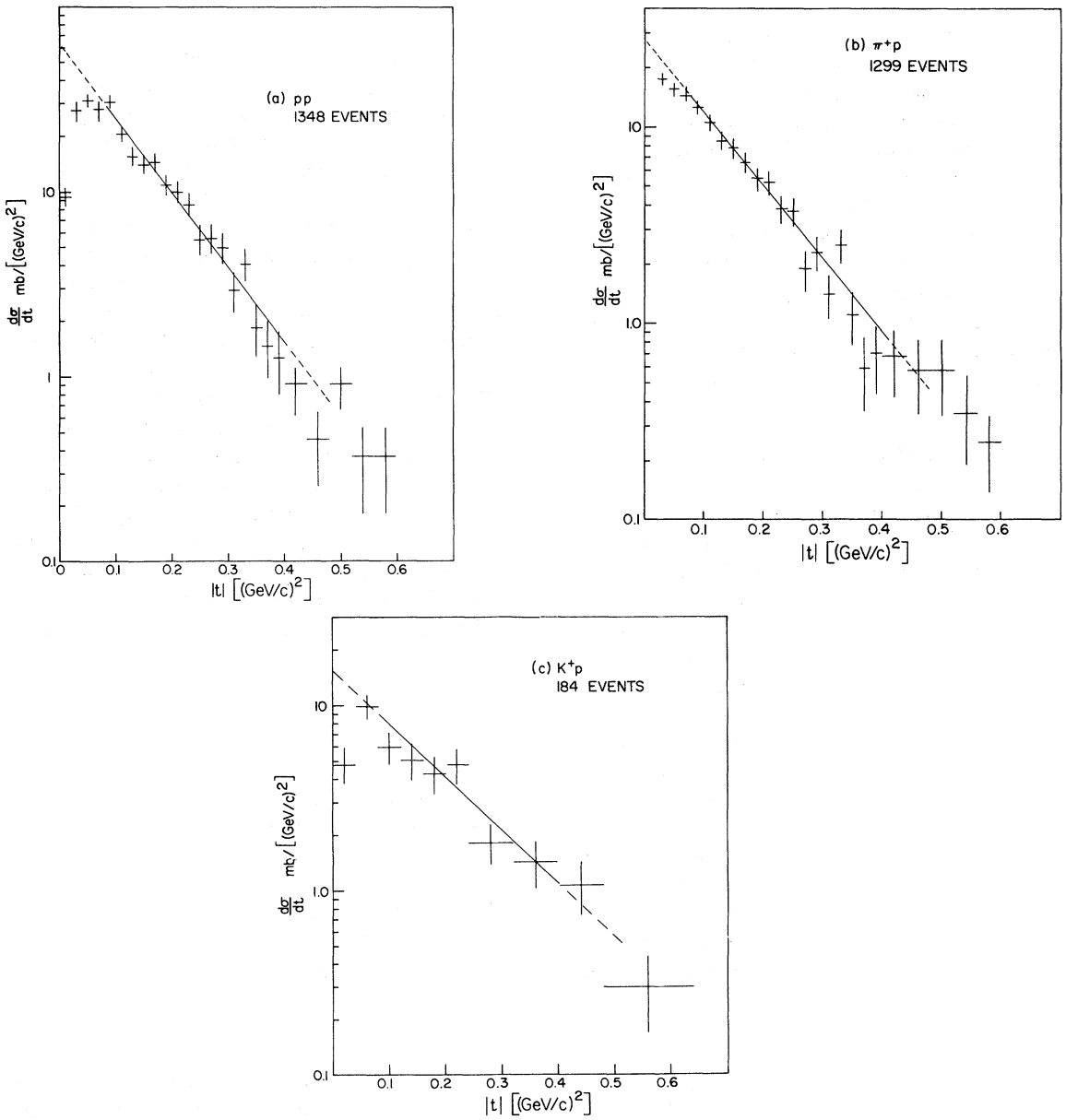


FIG. 2. $d\sigma/dt$ vs $|t|$, the four-momentum transfer for (a) *pp* interactions, (b) $\pi^+p$ interactions, and (c) $K^+p$ interactions. In each case the line is a fit to the points over the interval $0.08\leq|t|\leq0.40$ (GeV/$c$)$^2$ with the parameters given in Table II.

TABLE II. Elastic-scattering parameters.

| | $\sigma_{el}$ (mb) | Slope $[(GeV/c)^{-2}]$ | Optical point $[mb/(GeV/c)^2]$ | $\sigma_{tot}$ (mb) |
|---|---|---|---|---|
| $pp$ | | | | |
| This expt. | 6.85±0.24 | 9.2 ±0.5 | 63.0±5.7 | 38.47±0.58 |
| Refs. 10,11 | 6.99±0.08 | 10.38±0.17 | 76.3 | 38.62±0.06 |
| $\pi^+p$ | | | | |
| This expt. | 3.24±0.11 | 8.6 ±0.4 | 27.4±2.0 | 23.74±0.46 |
| Refs. 10,11 | 3.42±0.08 | 8.17±0.17 | 28.2 | 23.46±0.06 |
| $K^+p$ | | | | |
| This expt. | 2.37±0.22 | 6.5 ±1.0 | 15.2±2.7 | 19.52±0.52 |
| Refs. 10,11 | 2.43±0.09 | 7.61±0.28 | 19.2 | 19.33±0.08 |

exponential fits also yielded a value for $dN/dt \mid_{t=0}$ which was converted to cross section for the optical point $d\sigma/dt \mid_{t=0}$. These values also are listed in Table II. The value of the optical point determined here for $pp$ interactions is about 2 standard deviations lower than the value expected from the total cross section. However, the total elastic cross sections determined in this experiment are in excellent agreement with the results of Carroll *et al.*[10]

### B. Inelastic two-prong data and total cross sections

The events in the two-prong sample not flagged as elastics do not exhibit the same losses as the

TABLE III. Topological cross sections for $K^+p$ interactions.

| Number of charged prongs, $n_i$ | Observed number of events | | Corrected number of events | Cross section (mb) |
|---|---|---|---|---|
| 2 | 541 | | 706.9±40.4 | 4.31±0.25 |
| | | Elastic | 388.2±36.7 | 2.37±0.22 |
| | | Inelastic | 318.8±36.2 | 1.94±0.22 |
| 3 | 6 | | | |
| 4 | 545 | | 617.5±30.9 | 3.49±0.17 |
| 5 | 7 | | | |
| 6 | 560 | | 626.9±29.5 | 3.55±0.17 |
| 7 | 12 | | | |
| 8 | 540 | | 596.7±30.5 | 3.38±0.17 |
| 9 | 6 | | | |
| 10 | 418 | | 459.2±27.4 | 2.60±0.15 |
| 11 | 8 | | | |
| 12 | 197 | | 217.8±18.6 | 1.23±0.11 |
| 13 | 5 | | | |
| 14 | 94 | | 103.5±12.8 | 0.59±0.07 |
| 15 | 2 | | | |
| 16 | 39 | | 44.2±8.5 | 0.25±0.05 |
| 17 | 2 | | | |
| 18 | 12 | | 14.9±5.2 | 0.084±0.029 |
| 19 | 2 | | | |
| 20 | 4 | | 4.1±2.1 | 0.023±0.012 |
| 21 | | | | |
| 22 | 3 | | 3.2±1.8 | 0.018±0.010 |
| Total | 3003 | | | 19.52±0.52 |

TABLE IV. Topological cross sections for $\pi^+p$ interactions.

| Number of charged prongs | Observed number of events | | Corrected number of events | Cross section (mb) |
|---|---|---|---|---|
| 2 | 3828 | | 4768.0±111.4 | 5.26 ±0.12 |
| | | Elastic | 2940.4±97.6 | 3.24 ±0.11 |
| | | Inealstic | 1827.6±77.0 | 2.02 ±0.09 |
| 3 | 36 | | | |
| 4 | 3377 | | 3486.1±69.4 | 3.85 ±0.08 |
| 5 | 22 | | | |
| 6 | 3926 | | 3954.1±73.9 | 4.36 ±0.08 |
| 7 | 28 | | | |
| 8 | 3666 | | 3666.6±72.7 | 4.04 ±0.08 |
| 9 | 31 | | | |
| 10 | 2725 | | 2726.1±63.7 | 3.01 ±0.07 |
| 11 | 36 | | | |
| 12 | 1666 | | 1659.3±50.6 | 1.83 ±0.06 |
| 13 | 26 | | | |
| 14 | 794 | | 789.7±35.5 | 0.87 ±0.04 |
| 15 | 12 | | | |
| 16 | 381 | | 375.8±24.6 | 0.41 ±0.03 |
| 17 | 3 | | | |
| 18 | 132 | | 131.8±14.5 | 0.15 ±0.02 |
| 19 | 5 | | | |
| 20 | 38 | | 37.8±7.8 | 0.042 ±0.009 |
| 21 | 1 | | | |
| 22 | 11 | | 10.7±4.3 | 0.012 ±0.005 |
| 23 | | | | |
| 24 | 1 | | 1.0±1.0 | 0.0011±0.0011 |
| Total | 20745 | | | 23.74 ±0.46 |

elastics. Although not justified theoretically the inelastic $t$ distributions were fit to a single exponential form to get an estimate of the low-$t$ losses. These fits yielded slopes of $-4.4\pm0.6$ $(\mathrm{GeV}/c)^{-2}$, $-5.7\pm0.6$ $(\mathrm{GeV}/c)^{-2}$, and $-3.4\pm1.0$ $(\mathrm{GeV}/c)^{-2}$ with $\chi^2$/DF of 14.3/17, 13.8/15, and 6.9/8 for the $pp$, $\pi^+p$, and $K^+p$ interactions, respectively. These fits correspond to a 4% correction for missed $pp$ interactions, 5% for $\pi^+p$, and 7% for $K^+p$.

The remaining events, multiplicities $\geq 3$, for each beam type were then adjusted for the known losses. Using a density of liquid hydrogen of $0.0627 \pm 0.0005$ g/cm$^3$, the $40.5\pm0.2$ cm fiducial length, the total track count, and correcting for the attenuation of the beam through the bubble-chamber entrance window yields the $\mu$b/event equivalences

$$K^+p\text{: } 11.376\pm0.050\text{ ,}$$

$$\pi^+p\text{: } 2.036\pm0.005\text{ ,}$$

$$pp\text{: } 2.434\pm0.010\text{ .}$$

The addition of these cross sections to the inelastic two-prongs and the elastic-scattering cross sections yields the total cross sections listed in Table II. The errors quoted reflect the statistical uncertainties as well as an estimate of the systematic biases. The agreement with the results of Carroll *et al.*[10] is apparent.

## IV. TOPOLOGICAL CROSS SECTIONS AND MULTIPLICITY DISTRIBUTIONS

In order to improve the statistics of the high-multiplicity events, the data sample was enlarged to include events from rolls not used in the cross-section determinations. The enlarged sample consists of 3003 $K^+p$ interactions, 20745 $\pi^+p$ interactions, and 19410 $pp$ interactions. These numbers represent the largest data sample yet obtained for

TABLE V. Topological cross sections for $pp$ interactions.

| Number of charged prongs | Observed number of events | | Corrected number of events | Cross section (mb) |
|---|---|---|---|---|
| 2 | 4448 | | 5937.6±120.0 | 10.97 ±0.22 |
| | | Elastic | 3707.6±129.9 | 6.85 ±0.24 |
| | | Inelastic | 2230.0±119.0 | 4.12 ±0.22 |
| 3 | 23 | | | |
| 4 | 3383 | | 3481.0±68.2 | 6.43 ±0.13 |
| 5 | 18 | | | |
| 6 | 3757 | | 3758.7±71.1 | 6.94 ±0.13 |
| 7 | 34 | | | |
| 8 | 3015 | | 3016.5±64.8 | 5.57 ±0.12 |
| 9 | 24 | | | |
| 10 | 2139 | | 2143.8±55.6 | 3.96 ±0.10 |
| 11 | 36 | | | |
| 12 | 1340 | | 1333.3±44.4 | 2.46 ±0.08 |
| 13 | 16 | | | |
| 14 | 659 | | 654.9±31.6 | 1.21 ±0.06 |
| 15 | 9 | | | |
| 16 | 342 | | 335.1±22.5 | 0.62 ±0.04 |
| 17 | | | | |
| 18 | 119 | | 117.9±13.4 | 0.22 ±0.02 |
| 19 | 3 | | | |
| 20 | 30 | | 30.5±7.0 | 0.056 ±0.013 |
| 21 | 2 | | | |
| 22 | 8 | | 7.9±3.6 | 0.015 ±0.007 |
| 23 | | | | |
| 24 | 3 | | 3.0±2.0 | 0.0055±0.0037 |
| 25 | | | | |
| 26 | 2 | | 1.9±1.8 | 0.0035±0.0033 |
| Total | 19410 | | | 38.47 ±0.58 |

$K^+p$ and $\pi^+p$ interactions with incident beam momenta above 100 GeV/$c$.

### A. Corrections

A number of additional corrections are needed before a topological cross section can be computed. Most of these corrections are statistical redistributions of the events among multiplicities.

#### *1. Short stubs and close-in secondary interactions*

A little less than 1% (415 events) of the sample of 43 158 events had an odd number of prongs. Almost 42% of these odd-prong events had a Dalitz electron identified. The percentage varied from 11% for 3 prongs to 62% for 19 prongs. The other Dalitz electron being unidentified was counted as a secondary hadronic track. These fractions were used to distribute some of the odd prongs to the next-lower even multiplicity.

The remaining events in this category were due to either a missed short stub or an undetected secondary interaction. The region of obfuscation varied from approximately 0.5 cm for low-multiplicity events to about 2.5 cm for events with 10 prongs or more. The average number of prongs for the secondary interactions was 2.8. In addition, the observed number of secondary interactions increased with increasing multiplicity, not an unexpected result. The missed short stubs were the dominant cause for the "odd" prongs at low multiplicities as noted by missing positive charge. The remaining odd-pronged events were then distributed by moving events to the next-higher even multiplicity for a missed stub or lowering the multiplicities by one or three for the missed interactions. The multiplicities are insensitive to this redistribu-

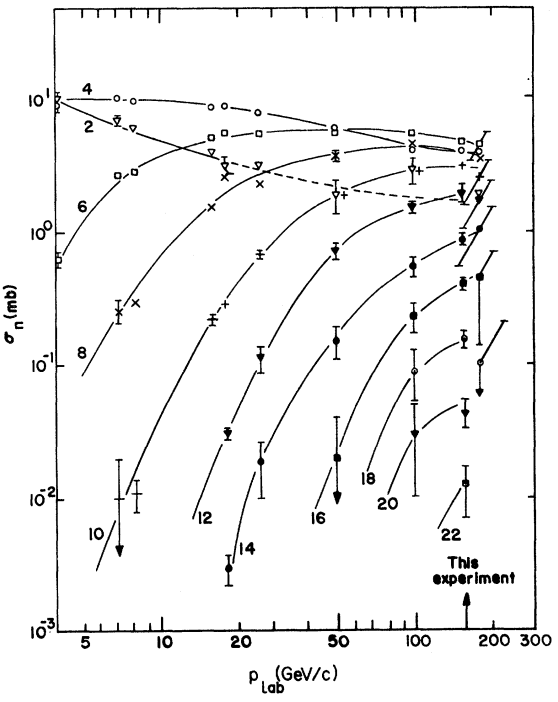


FIG. 3. Topological cross sections vs laboratory beam momentum for $\pi^+p$ interactions. The lines are to guide the eye.

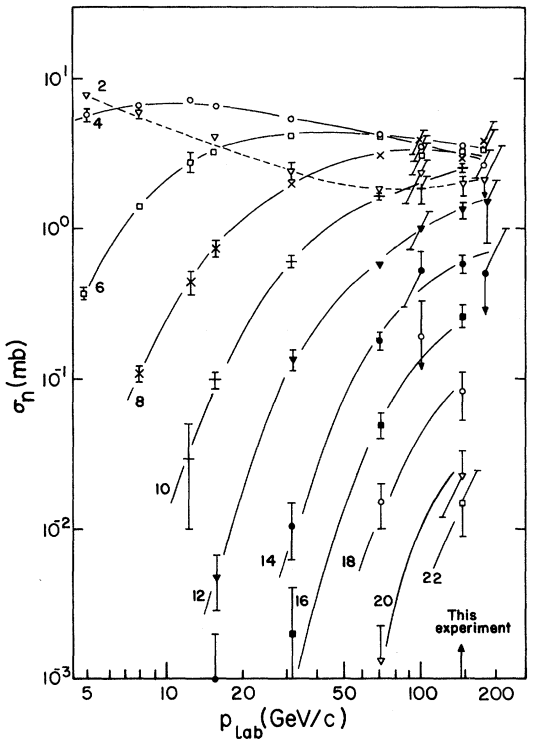


FIG. 4. Topological cross sections vs laboratory beam momentum for $K^+p$ interactions. The lines are to guide the eye.

tion since a 100% error in assignment of the short stubs and unseen interactions amounts to only a 0.2% change in any given topology.

### 2. *Unseen $V^0$'s and $\gamma$ conversions*

The confused vertex region leads, also, to a number of $V^0$ and $e^+e^-$ vertices not being resolved by the scan. Corrections were made to each beam type and multiplicity by shifting events to the next-lower even multiplicity on the basis of the estimated numbers missed.[12,13] Approximately 11% of these neutral vertices were estimated to be missed, affecting approximately 1.5% of all events.

### 3. *Unidentified Dalitz conversions*

The average number of $\pi^0$ mesons at each multiplicity for each beam type has been determined for two separate samples of data.[7,13] The number of Dalitz pairs was then estimated for each topology

TABLE VI. Multiplicity moments for $K^+p$, $\pi^+p$, and $pp$ interactions.

| Moment | Interaction $K^+p$ | $\pi^+p$ | $pp$ |
|---|---|---|---|
| $\langle n\rangle$ | 7.09±0.18 | 7.41±0.08 | 7.02±0.07 |
| $D=(\langle n^2\rangle-\langle n\rangle^2)^{1/2}$ | 3.48±0.14 | 3.60±0.06 | 3.65±0.05 |
| $\langle n\rangle/D$ | 2.03±0.10 | 2.06±0.04 | 1.92±0.03 |
| $f_2^{cc}=\langle n(n-1)\rangle-\langle n\rangle^2$ | 5.05±1.10 | 5.56±0.47 | 6.34±0.45 |

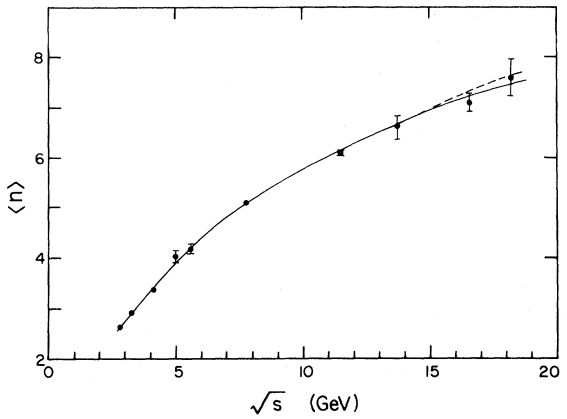


FIG. 5. Average charge multiplicity $\langle n \rangle$ as a function of the center-of-mass energy $\sqrt{s}$ for $K^+p$ interactions. See text for an explanation of the curves.

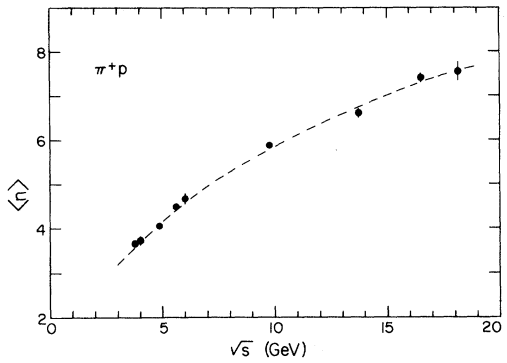


FIG. 6. Average charge multiplicity $\langle n \rangle$ as a function of center-of-mass energy $\sqrt{s}$ for $\pi^+p$ interaction. The dashed curve is a fit to the data (see text).

by using the branching ratio of 1.5%.[14] A total of 1360 Dalitz pairs is expected (3.2% of the events) but only one-third of these Dalitz pairs were identified. Corrections for the remaining unidentified Dalitz pairs were accomplished by the appropriate shifting of events from an even-number multiplicity to the next-lower even-numbered one.

### B. Topological cross sections

After adjusting the events as redistributed in Sec. IV A for scanning efficiencies, the samples were normalized to the elastic and total cross sections as determined in Sec. III. Table III lists the topological cross sections for $K^+p$ interactions, Table IV for $\pi^+p$ interactions, and Table V for $pp$ interactions. The errors quoted include an estimate of the systematic uncertainties as well as the statistical uncertainty. The errors on the elastic cross sections have been enlarged to incorporate the uncertainty in separation of the elastic from the inelastic two-prongs in addition to the large correction factors associated with the elastic events.

For $\pi^+p$ and $K^+p$ interactions the results of this experiment represent the highest-energy data, with excellent statistics, currently available. There now exist data for these reactions at 175 GeV/$c$ (Ref. 15) but with only 20% of the number of $K^+p$ interactions as here. These cross sections are displayed in Fig. 3 for $\pi^+p$ interactions with the results of lower-energy experiments.[16] The $K^+p$ cross sections are displayed in Fig. 4, again with the lower-energy data.[17] For each reaction the two-, four-, and six-prong cross sections are falling at the momentum of our experiment, the eight- and ten-prong cross sections have leveled out while the higher multiplicities are still rising with increasing beam momentum. We have chosen not to display the $pp$ cross sections since there exist very good data up to 400 GeV/$c$. The results determined here are consistent with the results of earlier data[18] on $pp$ multiplicities.

TABLE VII. Parameters of the energy-dependent fits to the average multiplicities.

| Parameters | $K^+p$ (1) | $K^+p$ (2) | $K^+p$ (3) | $\pi^+p$ (1) | $\pi^+p$ (2) | $\pi^+p$ (3) |
|---|---|---|---|---|---|---|
| $a$ | 0.92±0.17 | 1.37±2.58 | 2.38±0.04 | 1.57±0.31 | −1.9±5.8 | 2.53±0.18 |
| $b$ | 0.65±0.11 | 1.15±0.35 | 0.67±0.08 | 0.52±0.17 | 1.6±0.7 | 0.66±0.22 |
| $c$ | 0.08±0.02 | 1.71±1.61 | 0.41±0.03 | 0.09±0.02 | 4.9±1.9 | 0.40±0.06 |
| $d$ | | −2.32±1.81 | | | 0±4.9 | |
| $\chi^2$/DF | 0.97 | 0.77 | 0.90 | 2.4 | 2.7 | 2.22 |

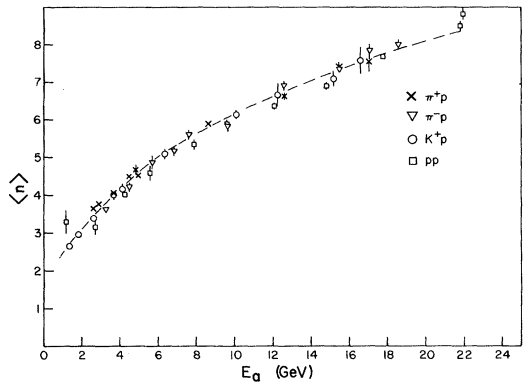


FIG. 7. Average charge multiplicity $\langle n \rangle$ as a function of the available energy, $E_a = \sqrt{s} - (m_{\text{beam}} + m_{\text{target}})$, for $\pi^+ p$, $K^+ p$, and $pp$ interactions. See text for an explanation of the curve.

### C. Multiplicity moments

Some of the moments of the multiplicity distributions for each beam are given in Table VI. The average charged multiplicity $\langle n \rangle$ is compared to lower-energy data for $K^+ p$ in Fig. 5. In general, the results extrapolate nicely from the lower-energy data. Here $\langle n \rangle$ has been plotted against the center-of-mass energy $\sqrt{s}$ instead of the more usual $p_{\text{lab}}$ in order to accentuate the differences in the fits attempted. A fit of the form $\langle n \rangle = a + b \ln(s/s_0)$ where $s_0 = 1$ GeV$^2$ yields an unacceptably large $\chi^2/\text{DF} = 4.17$. We have attempted to fit three differing types of expressions,

$$\langle n \rangle = a + b \ln(s/s_0) + c[\ln(s/s_0)]^2 , \quad (1)$$

$$\langle n \rangle = a + b \ln(s/s_0) + c(s/s_0)^{-1/2} + d(s/s_0)^{-1/2} \ln(s/s_0) , \quad (2)$$

$$\langle n \rangle = a + b \ln(E_a/E_0) + c[\ln(E_a/E_0)]^2 , \quad (3)$$

where $E_a = \sqrt{s} - (m_{\text{beam}} + m_p)$ is the available energy in the center-of-mass system as suggested by Whitmore[16] and $E_0$ is taken to be 1 GeV. The parameters for these fits are given in Table VII. Fit (2) is superimposed on Fig. 5 as the solid curve with fit (1) as the dashed portion where the two results differ. Either one describes the data adequately.

The average multiplicity for $\pi^+ p$ interactions is shown in Fig. 6 as a function of $\sqrt{s}$. The same expressions used for the $K^+ p$ data were fit here with the results given in Table VII. Although large, the $\chi^2/\text{DF}$ are reasonable considering the small errors (typically 0.01 to 0.04) associated with these averages. The result of fit (1) is superimposed on these data. The values for the fit using the available energy $E_a$ for each reaction are in remarkable agreement with the values found by Whitmore[16] for $\pi^- p$ and $pp$ interactions. Performing a simultaneous fit of $\langle n \rangle$ vs $E_a$ for $\pi^+ p$, $\pi^- p$, $K^+ p$, and $pp$ interactions over the range of laboratory momenta from 3.5 to 405 GeV/$c$ (Refs. 15–19) yields

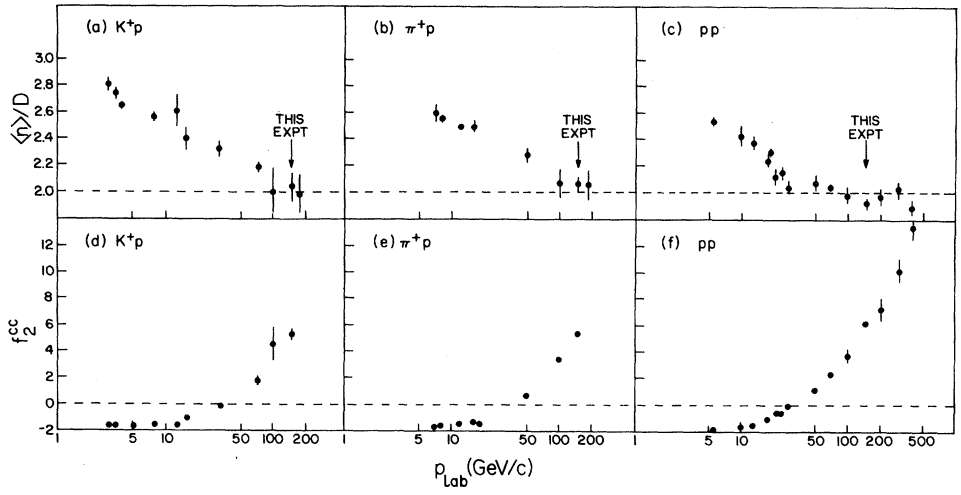


FIG. 8. $\langle n \rangle$/dispersion for (a) $K^+ p$, (b) $\pi^+ p$, (b) $\pi^+ p$, and (c) $pp$ interactions as a function of incident beam momentum. The dashed line is the expected value for KNO scaling. The correlation parameter $f_2^{cc}$ as a function of incident beam momentum for (d) $K^+ p$, (e) $\pi^+ p$, and (f) $pp$ interactions.The dashed line corresponds to a Poisson distribution.

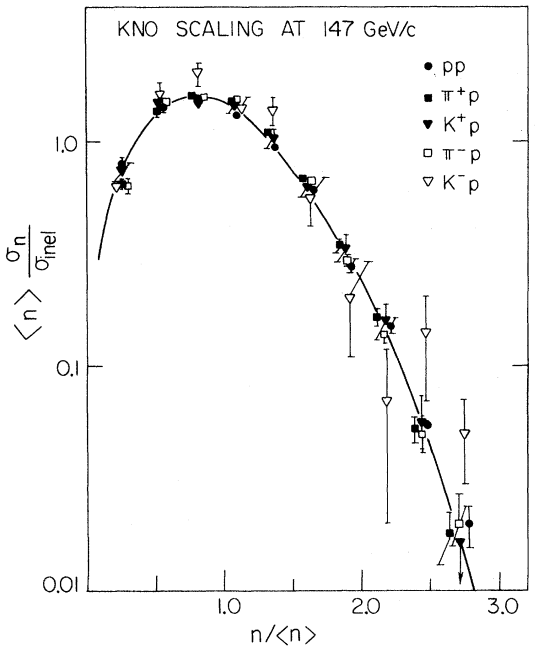


FIG. 9. The KNO scaling function $\langle n \rangle \sigma_n / \sigma_{\text{inel}}$ vs $n/\langle n \rangle$ for interactions at 147 GeV/$c$. The curve is from Ref. 23.

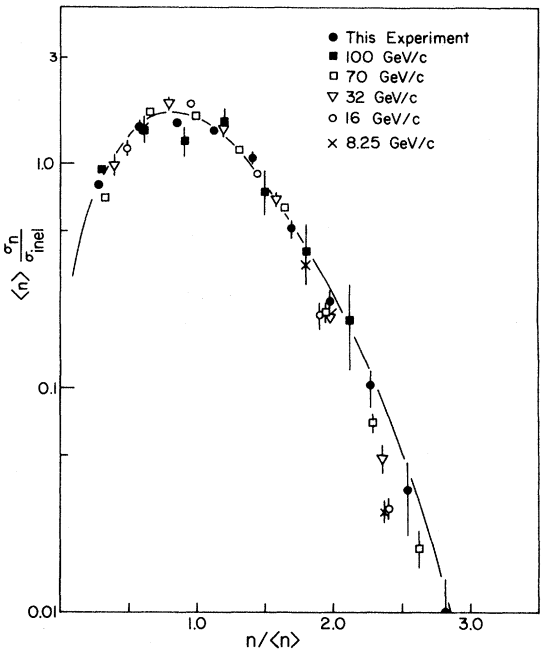


FIG. 10. The KNO scaling function $\langle n \rangle \sigma_n / \sigma_{\text{inel}}$ vs $n/\langle n \rangle$ for $K^+p$ at various beam momenta as indicated. The curve is from Ref. 23.

$$\langle n \rangle = (2.41 \pm 0.05) + (0.69 \pm 0.07) \ln(E_a/E_0) + (0.40 \pm 0.02)[\ln(E_a/E_0)]^2$$

which is displayed, superimposed on the data, in Fig. 7. The result is insensitive to the error assignments on the data in that the introduction of a 1% error as a floor on $\langle n \rangle$ reduced the $\chi^2$ by a factor of 5 while the fitted parameters remained within 1 standard deviation of the values given.

The $\pi^+p$-$pp$ charged-multiplicity difference is found to be $\langle n \rangle_{\pi^+p} - \langle n \rangle_{pp} = 0.39 \pm 0.11$ which is in excellent agreement with the difference of 0.33 calculated by Cirit[20] using a dressed-quark model. The $K^+p$-$pp$ charged-multiplicty difference is $\langle n \rangle_{K^+p} - \langle n \rangle_{pp} = 0.07 \pm 0.10$. Although this difference is not inconsistent with the value of 0.33, it continues the trend for the $K^+p$ interactions observed at lower momenta[21] where $\langle n \rangle_{K^+p}$ is closer to $\langle n \rangle_{pp}$ than $\langle n \rangle_{\pi^+p}$. Whether this behavior is due to the strange quark or to the energy dependence is unresolved.

The remaining two principal moments of the multiplicity distributions are shown in Fig. 8 with the results from the other experiments.[15–19] The broadening of the multiplicity distributions as indicated by the rise in the quantity $f_2^{cc}$ is apparent. This is not surprising since the ratio $\langle n \rangle / D$ has decreased with increasing beam momentum. For the $\pi^+p$ interactions, Fig. 8(b), the ratio $\langle n \rangle / D$ appears to be leveling at a value near but slighlty larger than 2 compared to a value of slightly less than 2 for the $pp$ interactions.[16] A similar leveling may be occurring for the $K^+p$ interactions, Fig. 8(a), with $p_{\text{lab}} \geq 100$ GeV/$c$ although a continuing decrease in $\langle n \rangle / D$ with increasing $p_{\text{lab}}$ cannot be ruled out.

### D. Scaling

If the ratio $\langle n \rangle / D$ is approaching an asymptotic value then the data of this experiment should exhibit the form for exact Koba-Nielsen-Olesen (KNO) scaling.[22] In Fig. 9 we have plotted the results of this experiment and of the companion negative beam experiment[2] in terms of the scaling variables. The five reactions are similar to each other and follow closely Slattery's empirical fit[23] to the data for $pp$ collisions between 50 and 300 GeV/$c$ (solid curve). This approach to scaling can be seen in Fig. 10 where $K^+p$ topological cross sections for

various beam momenta are displayed. Only the data from 100 and 147 GeV/$c$ agree with the empirical fit at high multiplicities while the data from lower momenta show marked deviations in this region.

## ACKNOWLEDGMENTS

We are pleased to acknowledge the assistance of the Fermilab 30-in. bubble-chamber staff and members of the Neutrino Section during the course of this experiment. We appreciate the effort and diligence of the technical staffs at the many institutions involved to acquire the data presented. This work was supported in part by the U. S. Department of Energy, the National Science Foundation, the Israeli Academy of Sciences (Commission for Basic Research), the U. S.-Israel Binational Science Foundation, the Dutch Stichting voor Fundamental Onderzoek der Materie and the Italian Instituto Nazionale di Fisica Nucleare.

---

*Present address: University of Liverpool, Liverpool, England.
†Present address: Université de Neuchatel, Neuchatel, Switzerland.
‡Present address: Duke University, Durham, North Carolina 27706.
§On leave of absence from University of Pavia, Pavia, Italy.
‖On leave of absence from Institute of High Energy Physics, Beijing, China.
¶Present address: Collège de France, Paris, France.
**On leave of absence from Nara Women's University, Nara, Japan.
††Present address: Automatix, Burlington, Massachusetts 01803.
‡‡Permanent address: Seton Hall University, South Orange, New Jersey 07079.
§§Present address: Brookhaven National Laboratory, Upton, New York 11973.

[1]D. Brick *et al.*, in *Proceeding of the International Symposium on Recent Bubble Chambers Physics, Tohoku University, 1978*, edited by S. Tanaka (Tohoka University, Sendai, Japan, 1979) p. 99; E. B. Brucker *et al.*, Bull. Am. Phys. Soc. 23, 634 (1978).
[2]D. Fong *et al.*, Nucl. Phys. B102, 386 (1976).
[3]M. Heller *et al.*, Nucl. Instrum. Methods 152, 379 (1978).
[4]W. W. Neale, Fermilab Report No. FN-259, 1974 (unpublished).
[5]J. Lach and S. Pruss, Fermilab Report No. TM-298, 1971 (unpublished).
[6]H. Rubin and T. Ludlam, Proportional Hybrid Spectrometers Consortium Newsnote No. 40, 1975 (unpublished).
[7]A more detailed presentation of the filtering may be found in B. M. Whyman, Ph.D. dissertation, University of Cambridge, 1980 (unpublished).
[8]International Hybrid Spectrometer Consortium Newsnote No. 41, 1977 (unpublished).
[9]Hydra Applications Manual, CERN EP Division.
[10]A. S. Carroll *et al.*, Phys. Rev. Lett. 33, 932 (1974); 33, 928 (1974).
[11]D. S. Ayres *et al.*, Phys. Rev. D 15, 3105 (1977).
[12]L. Bachman, Ph.D. dissertation, The Johns Hopkins University, 1979 (unpublished) and private communication.
[13]D. Brick *et al.*, Nucl. Phys. B164, 1 (1980).
[14]Particle Data Group, Phys. Lett. 75B, 1 (1978).
[15]Fermilab Single Arm Spectrometer Group, A. Aitkenhead *et al.* (unpublished).
[16]J. Whitmore, Phys. Rep. 10C, 273 (1974); 27C, 187 (1976), and references therein.
[17]M. Barth *et al.*, Z. Phys. C 2, 285 (1979) and references therein for lower-energy data.
[18]For these comparisons see Refs. 1 and 7.
[19]For data to 16 GeV/$c$, see V. V. Ammosov *et al.*, Nucl. Phys. B58, 77 (1973); 18.5 GeV/$c$, J. T. Powers *et al.*, Phys. Rev. D 8, 1947 (1973); 50 GeV/$c$., G. A. Akopdjanov *et al.*, Nucl. Phys. B75, 401 (1974); 100 GeV/$c$, W. M. Morse *et al.*, Phys. Rev. D 15, 66 (1977); 175 GeV/$c$, Ref. 16.
[20]M. A. Cirit, Phys. Lett. 82B, 123 (1979).
[21]A. R. Erwin *et al.*, Phys. Rev. Lett. 36, 637 (1976) and W. M. Morse *et al.*, Phys. Rev. D 15, 66 (1977).
[22]Z. Koba *et al.*, Nucl. Phys. B40, 317 (1972).
[23]P. Slattery, Phys. Rev Lett. 29, 1624 (1972).